V International Conference on Particle-based Methods – Fundamentals and Applications
PARTICLES 2017
P. Wriggers, M. Bischoff, E. Oñate, D.R.J. Owen, & T. Zohdi (Eds)

AN APPROACH TO DEM MATERIAL CHARACTERIZATION IN COHEISVE GRANULAR BULK SOLID MATERIALS

LIZ I. DEL CID[1] AND AJITH SUBRAMANIAN[2]

[1,2]Overland Conveyor Company, Inc.
ThyssenKrupp Industrial Solutions, USA
1536 Cold Blvd, Bldg. 4 Suite 150
Lakewood, Colorado, USA 80401
[1]LDelCid@overlandconveyor.com, [2]AjithSub@overlandconveyor.com
http://www.overlandconveyor.com/

Key words: Granular Materials, DEM, Angle of Repose, Cohesion, Contact Problems.

Abstract. In bulk handling applications, such as conveying and storage, understanding the DEM particle characteristics to best simulate the flow of particulate systems at the macroscopic scale addresses an uncertainty in the DEM simulation of operational unit design and handling scenarios. This research provides a better understanding of the role adequate DEM material properties have on the flow-ability of bulk solid materials through the development, implementation and application of a generic material model procedure used in developing DEM input properties from physical testing data. This investigation proposes coupling physical material testing procedures with a DEM history dependent particle-particle macroscopic elasto-plastic adhesive contact model that accounts for both elastic and plastic contact deformations and cohesive attractions [1, 2]. The research application tasks are focused on three major areas: 1) measure a bulk solid's cohesive and frictional properties under mass flow and pressure, 2) simulate each material sample through a series of test controlled standards, 3) verify the suitable predicted material properties in the test applications simulate and are comparable to experimental results. As part of physical testing, such simulations can be used as part of the optimization for bulk handling design and operation.

1 INTRODUCTION

The interactions between granular bulk material and machinery plays an important role in our mining industry. A promising model of these interaction comes from the discrete element method. The difficulty with DEM however, is determining the behavioral flow of the macro material from the material micro-properties. In DEM, each particle has material parameters that influence the particle and its bulk behavior (e.g. spring stiffness, friction coefficients, damping values, bonding strength). Laboratory experiments and in-situ tests are necessary to determine these properties before any useful modelling can be performed. Developing methods to accurately calibrate and numerically quantify the bulk mechanical behavior of granular materials from measured properties is a formidable task [3-5]. Even then, the resulting simulations and the validity of the measured parameters is not without uncertainty.

The objective of this study is to develop a calibration process in which the DEM material parameters can be determined. For this purpose, experimental and DEM results from shear tests and industry field tests are used.

2 NUMERICAL MODELING USING A MACRO ELASTO-PLASTIC ADHESIVE (MEPA) MODEL

The contact model used in this study follows the MEPA cohesive model implementation for stress history dependency. The MEPA model is a three branched non-linear contact model that simulates the elastic and plastic regimes of particulate solids. It is capable of modeling material yielding through hysteresis and steady-state flow. This section describes the approach to the contact duration with cohesive attraction for each particle contact.

2.1 The MEPA Cohesive Model

The MEPA model uses a maximum force-based failure criterion. It determines the maximum displacement of the contact with a material stiffness described by the material's tensile strength, elastic modulus and Poisson's ratio. This model is used to simulate the mechanical behavior of material physical data in a shear test rather than the micro and molecular mechanics laws. It simulates the results from the physical testing used to determine the parameters of the Mohr-Coulomb shear failure criterion and complements studies in cohesive, frictional bulk solids for micro- and macro-models of different materials [6-12].

2.2 Particle Contact Constitutive Model

The relationship between the interaction force and the normal overlap of two rigid DEM particles is shown in Figure 1. The loading, unloading/re-loading and cohesive branches in the MEPA model are represented by four parameters: the virgin loading stiffness parameterk_1, the unloading and reloading stiffness parameter k_2, the cohesive stiffness parameter k_{adh} and the index parameter n, controlling the nonlinear force-displacement response of the system [9-11]. In the initial loading of the contact, the force increases with stiffness k_1. A linear viscous damping dash-pot is used to dissipate energy during contact. Cohesion between the contacts is represented by cohesive stiffness k_{adh}, which allows for attraction forces controlled by a limiting force f_{min}. Note, when n = 1, the model becomes linear and is represented by the branched model of Figure 1a. If k_1 is set equal to k_2, the model is reduced to the linear or Hertzian contact model previously discussed. Each branch can be expressed by the following sets of bounding equations:

$$f_1(\delta) = k_1\delta^n \tag{1}$$

$$f_2(\delta) = k_2\left(\delta^n - \delta_p^n\right) \tag{2}$$

$$f_3(\delta) = -k_{adh}\delta^n \tag{3}$$

where $f_1(\delta)$ represents the virgin loading branch, $f_2(\delta)$ the re/unloading branch, and $f_3(\delta)$ the cohesive branch. The branched relationship as a whole can be expressed as:

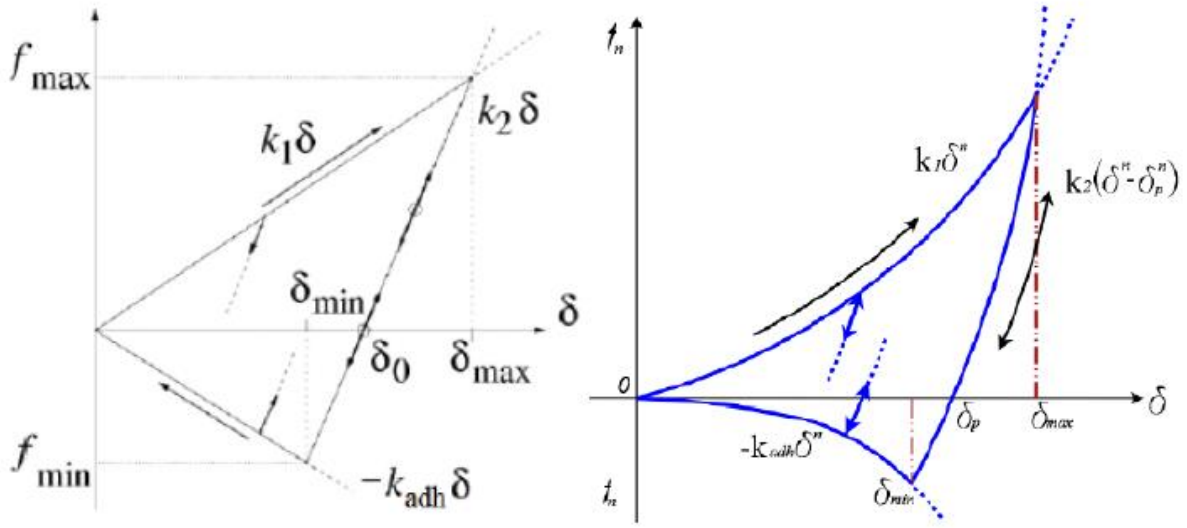

(a) Linear MEPA cohesive contact law. (b) Non-linear MEPA cohesive contact law.

Figure 1: Different MEPA contact models from [13].

$$f_{hys} = \begin{cases} f_1(\delta) & if \quad f_2(\delta) \geq f_1(\delta) \\ f_2(\delta) & if \quad f_1(\delta) > f_2(\delta) > f_3(\delta) \\ f_3(\delta) & if \quad f_3(\delta) \geq f_2(\delta) \end{cases} \tag{4}$$

The normal force on particle i is described by:

$$\boldsymbol{f}_0^n = -\gamma_n \boldsymbol{v}_n + f_{hys}\boldsymbol{n} \tag{5}$$

with the normal direction unit vector $\hat{n}$ directed from the center of particle j to particle i. The variable $\boldsymbol{v}_n$ describes the normal relative velocity of the particle and γ_n the viscous dissipation coefficient. The tangential force includes dissipation due to Coulomb friction and tangential elasticity that allows for stick-slip behavior at the contact level [6, 11-12]. The tangential force is related to the normal force via Coulomb's law in equation 6.

$$f^t \leq \mu_s f_{hys} \tag{6}$$

The maximum adhesion is determined by the stiffness parameters and the maximum normal overlap f_{max}. The tangential stiffness is calculated based on the contact stiffness k_t, which is set to the value of k_1. The tangential force is calculated from the product of the tangential stiffness and the tangential displacement, subject to the frictional limit according to Coulomb's law. At the maximum contact overlap, f_{max}, the contact stiffness increases instantaneously to the value k_2. Further loading and unloading is defined by the force-displacement relation $f = f_2(\delta)$. Elastic unloading to a zero contact force leads to a non-zero contact overlap equal to the maximum plastic contact indentation, $\delta = \delta_p$, which is recorded and updated over the contact lifetime. When the contact overlap is further decreased as the

particles separate, the contact force enters the tensile regime. The maximum tensile contact force $f = -k_{adh}\delta_{min}^{n}$ that the contact can experience corresponds to a contact displacement $\delta = \delta_{min}$. Further unloading in the tensile regime generates a tensile contact force that decreases in accordance with $f = -k_{adh}\delta$. In addition to the loading and unloading branches shown in Figure 1a and b, loading and unloading may also occur within the bounding branches. Any loading stage within the bounding branches loads or unloads elastically in accordance with $f = f_2(\delta)$ [14].

3 SETUP OF CALIBRATION PROCEDURE

To provide the experimental shearing data of the material under various conditions, the laboratories of Jenike & Johanson are used. To assist in the calibration of numerical parameters required for DEM simulations a set of in situ materials tests are also performed. The material properties should represent a range of possible operating conditions, as used in the design process. These standards will be inferred to be applicable by choice of and referenced by the test laboratory. A secondary purpose of the testing is for the DEM analyst to understand unique properties of the materials outside of the tests described that might impact the behavior of the bulk material.

3.1 Material Preparation

Proper collection of data for DEM simulations starts with a representative collection of the sample material. Figure 2 shows an example of material pulled from a transfer line and has been dried before proceeding. The bulk material is further sieved for size distribution and conditioned for uniformity of testing. All material smaller than ~1.5mm is set aside and not included in further testing.

Figure 2: Images of received material (Waste Rock and Clay Ore)

3.2 Density Testing

The density of the test samples is evaluated using containers having a minimum minor dimension of 10x the median particle for each sample. The container is filled through a sieve

approximately 2x the median size and weighed after filling without vibration or jostling. The container with material is weighed and the internal dimensions of the container measured to calculate the volume. The average density is defined as the total material mass divided by the volume filled by the material [15].

In the simulation, the assembly of particles is given an initial density and the system allowed to reach static equilibrium. The density is calculated in the same manner as the physical test. Using an iterative approach, the DEM particle density is modified until the average density is representative of the measured value.

3.3 Wall Friction

The preferred method of measuring the wall friction is with a modified shear cell with a minimum dimension of 5x the median particle. A bed depth of at least 3x the median particle is used to limit rotation. If a shear cell is used, tests will be made with pressures up to the equivalent hydrostatic pressure of approximately 50x the median particle deep.

In situ test cases where a layer of a single particle deep slides on an inclined plane without rolling, the wall friction is determined as the tangent of the wall angle determined from an inclined plane test procedure as shown in figure 3.

(a) Image of netting for wet bulk sliding.

(b) DEM vector simulation for the sliding friction analysis of wet clay ore.

Figure 3: Lab image of wall friction lab and DEM simulation setup.

In the simulation, the particles are initially at rest as the plane increases in angle from the horizontal. The velocity vector of the particles are tracked and the wall friction angle calculated as the angle upon which the velocity vector of the particles is no longer moving with the plane and the angular velocity is still zero indicating slip condition only.

3.4 Rotational Resistance

Rotational resistance is tested on an inclined plane test stand. If the particles roll before sliding on an inclined chute material, the sliding will have to be determined with a shear cell test and the rolling resistance is determined with an inclined test on the wall material sample. If it is necessary to prevent particle sliding on an inclined plane the rolling resistance is tested with an otherwise smooth surface equipped with lateral rows of wire of diameter ~20% of the

median particle size spaced at 2x the particle median size. Alternatively, a machined saw tooth surface of the same dimensions oriented to resist sliding is used.

In the simulation, the particles are initially at rest as the plane increases in angle from the horizontal. The angular velocity of the particles are tracked and the rotational resistance coefficient calculated as the angle upon which the angular velocity of the particles is non-zero.

3.5 Angle of Repose

A conical angle of repose test as described in the CEMA 550 with a rough base is used to characterize the bulk material flow potential. For the DEM simulation, the geometry is scaled to the selected particle size accordingly. Figure 4 displays pile formations obtained following the testing standard.

(a) Dry waste rock pile formation (b) Wet clay ore file formation

Figure 4: Lab image of angle of repose pile formation for dry and wet waste rock and clay.

Figure 5 demonstrates the DEM simulation iterations of the same simulated procedure as the sliding inter particle friction coefficient increases. The number of iterations required depends on the accuracy desired and the initial friction coefficient range. Typically 6 iterations are performed with dry loose material under a one degree tolerance of the measured angle of repose. Figure 6 displays the measurement made by the DEM simulation when the system has reached static equilibrium.

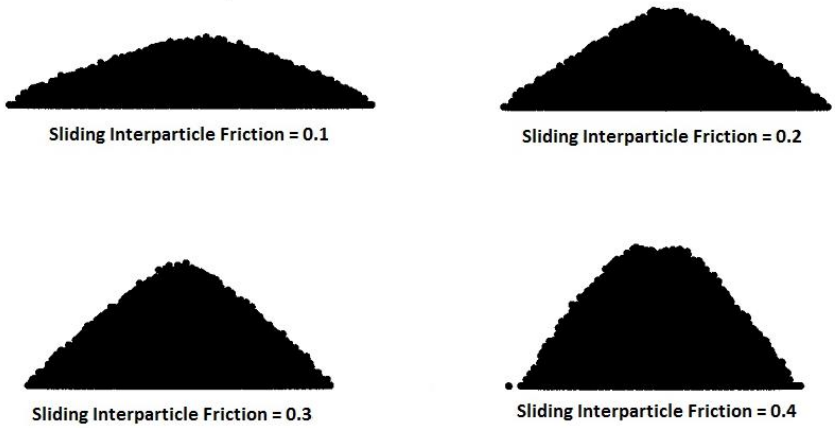

Figure 5: Angle of repose iterations of simulated material.

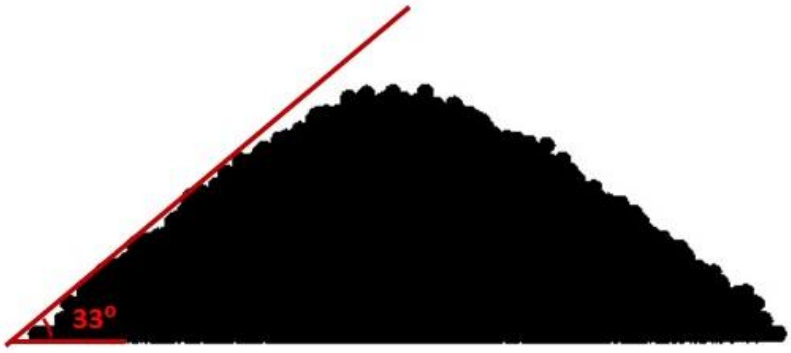

Figure 6: Angle of repose of final material simulation.

3.5 Physical Translational Shear Tester

The physical shearing test performed uses the Jenike Shear Tester, a translational shear tester. The shear cell is composed of a base located on the frame of the shearing machine. A ring rests on top of the base with a cover or lid. The surface conditions of the bottom of the cover and the inside of the base are rough to increase adhesion of the tested solid. The material is loaded into the base and ring and then covered. A normal force, F_N is applied centrally on the cover and held. The upper part of the shear cell is displaced horizontally against the fixed bottom base by a stem. The measured value is the shearing force exerted by the stem [16]. The normal stress, σ, and the shear stress, τ, acting in the horizontal plane between the top and bottom rings are determined by dividing the normal force, F_N; and shear force, F_S, by the cross-sectional area of the shear cell, A. The standard shear cell is 95.25 mm in diameter with a shearing rate of 4:487 x 10^{-5} $\frac{m}{sec}$ [16, 17]. A schematic of the physical tester with the dimensions defined in millimeters is shown in figure 7.

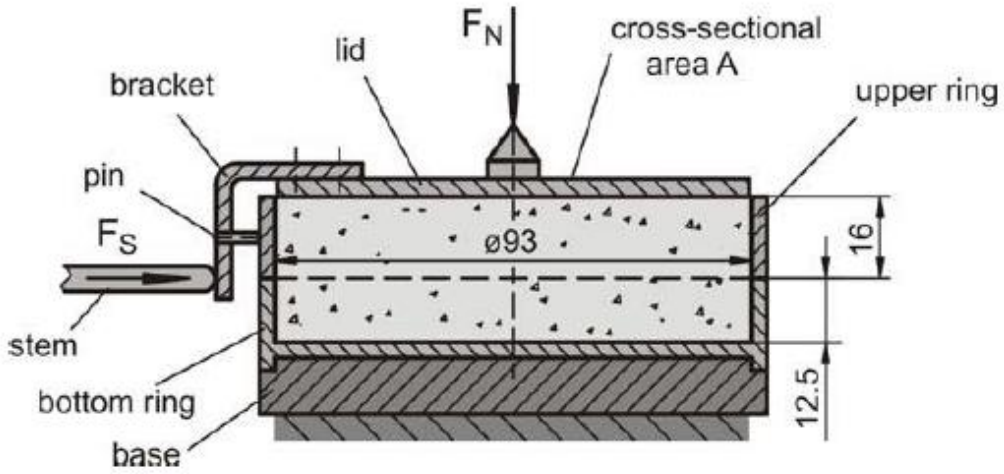

Figure 7: Jenike and Johanson direct shear test schematic from [16].

In the simulation, the experimental data sets are obtained with the ring cell shear tester developed by Dietmar Schulze [18, 19] are used to minimize localized stresses. Figure 8

shows a schematic of a ring shear tester series RST-01 [16, 18-20]. The ring-shaped bottom ring of the shear cell contains the material sample, while the lid is placed on top of the material and fixed at a crossbeam. A normal force is exerted to the crossbeam in the rotational axis of the shear cell and transmitted through the lid to the material sample. The counterbalance force, F_A, acts in the center of the crossbeam and counteracts the gravity forces of the lid, the hanger, and the crossbeam [16]. To shear the sample, the lid and the bottom ring of the shear cell rotate relative to each other. This is achieved by rotating the bottom ring while the lid and the crossbeam are prevented from rotating by the connecting tie-rods. Each of the tie-rods are fixed at a load-beam from which the forces acting on cell can be measured. The test procedure is comparable to the one performed by the Jenike shear tester. The yield locus from the measured shear points as per the physical test procedure. Modeling the consolidation of material with time history is the advantage of using the MEPA model as the particle contact model.

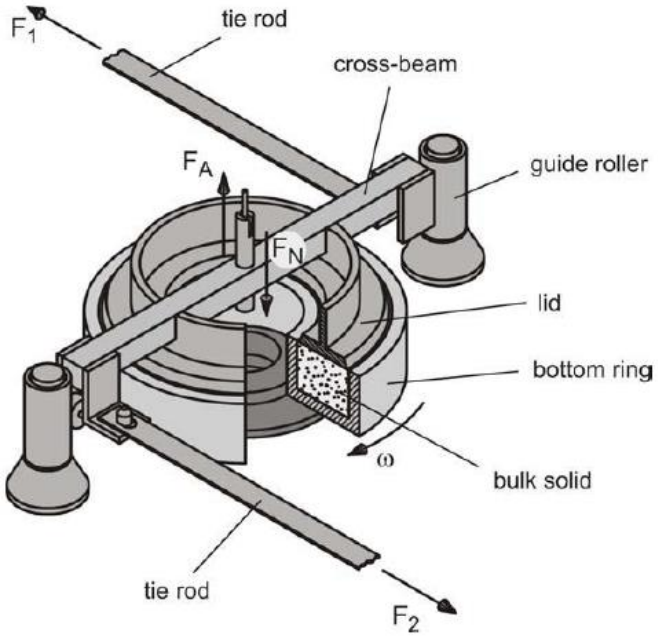

Figure 8: Shear Cell of a ring shear tester type RST-01 from [16, 18-20].

4 BULK MATERIAL PROPERTIES DETERMINATION

This procedure to DEM material characterization has been used for dry material over a number of industry projects. Cohesive materials provide the greatest uncertainly in material flow behavior. For this investigation various tests were conducted on wet copper ore with a top size of 7 mm. The simulation involved evaluating the particle size distribution seen in figure 9. Some of the experimental parameters are listed on Table 1. The boundary material for static wall friction testing #2B finish stainless steel sheet. An image of the copper ore material is shown in figure 10.

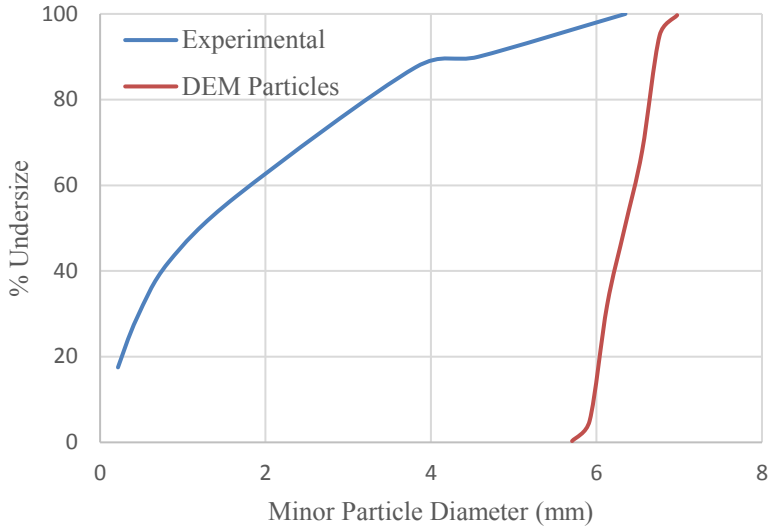

Figure 9: Particle size distribution of copper ore.

(a) Physical copper ore material at 8% mc (b) Virtual DEM copper ore material at 8% mc.

Figure 10: Lab and DEM simulation image of the sample material copper ore at 8% moisture content.

Table 1: Measured properties of iron ore

Parameter	value
Particle Density, ρ_s $(kg\ m^{-3})$	2481.3
Bulk Density, ρ_{bl} $(kg\ m^{-3})$	1042.8-1752.4 (5% wb moisture content)
Bulk Density, ρ_{bl} $(kg\ m^{-3})$	1350.4-1797.3 (8% wb moisture content)
Internal Frictional Angle, φ (degrees)	47.3 (5% wb moisture content)
Internal Frictional Angle, φ (degrees)	46.7 (8% wb moisture content)
Wall Friction Angle, φ (degrees)	30.0 (5% wb moisture content)

5 RESULTS AND DISCUSSION OF DEM MATERIAL CHARACTERIZATION

The approach to characterizing cohesive copper ore started with lab tests, which provided the parameters values of Table 1 and the failure envelopes for a range of conditions. To begin, the young's modulus was set to known values for copper ore, approx. 113-119 GPa with a

Poisson's ratio of 0.34. These parameters governed the stiffness, k_1 and k_2, values of the elasto-plastic model. The inter-particle friction and cohesive stiffness were adjusted to simulate the experimental measured profile of the Mohr Coulomb failure criteria. For copper ore with 5% moisture content, figure 11 displays the data the DEM simulation was to closely match. The inter particle friction and cohesive stiffness used came to 0.35 and $k_{adh} = 3.56x10^8 \frac{N}{m}$ respectively. Figure 12 displays the resulting DEM profile of this condition.

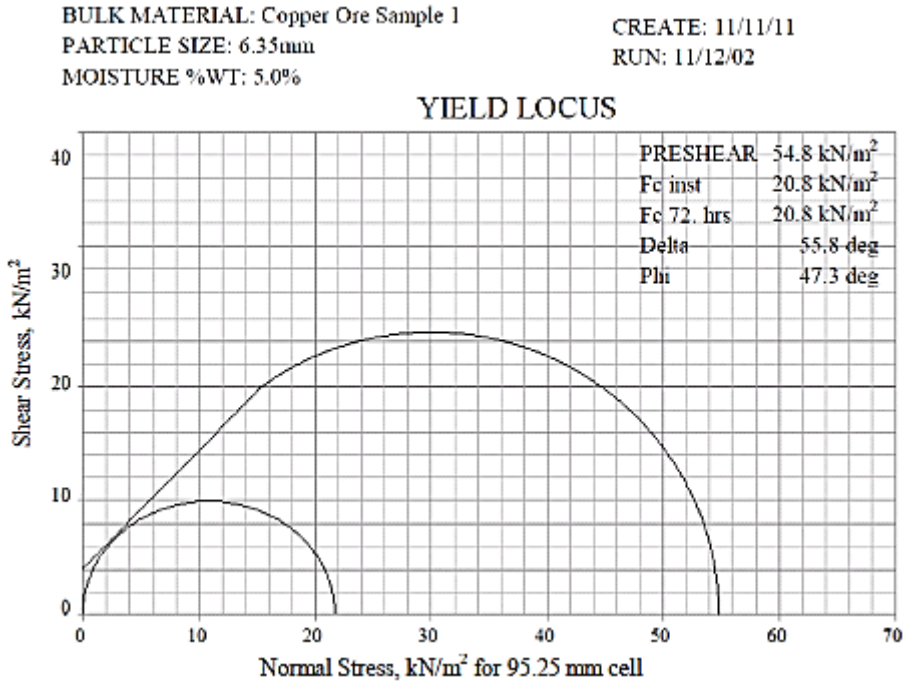

Figure 10: Physical testing results of the loading for Copper Ore Sample 1 at 5% mc.

The angle of repose simulation was not performed as this test has a greater uncertainty with highly cohesive materials. However, the wall friction test using the inclined plane simulation was performed and a frictional coefficient value of 0.7 was observed resulting in a wall frictional angle of 35 degrees ± 3 degrees. The number of iterations performed was not sufficient to more closely simulate the laboratory findings. Table 2 summaries the DEM parameters determined through the simulation of the laboratory tests. Utilizing the parameters determined for copper ore, the agglomeration of the physical material can be observed in the virtual DEM simulated material as seen in figure 10. To perform a through calibration requires computation time and human resources. For this material set, a loose tolerance was acceptable to minimize project cost.

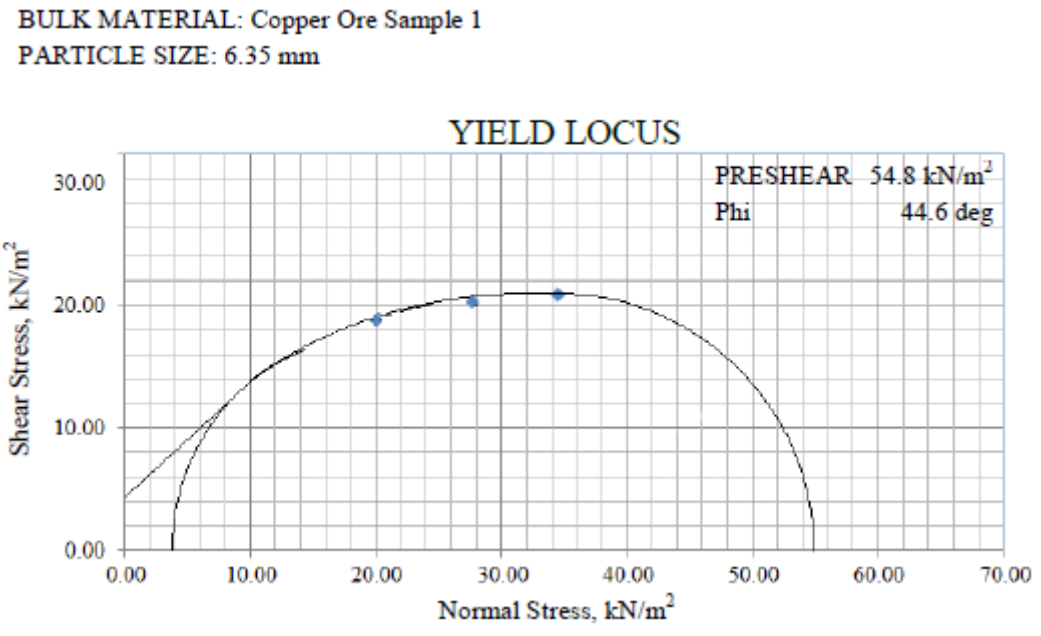

Figure 11: Simulated testing results of the loading for Copper Ore Sample 1 at 5% mc.

Table 2: Simulated properties of iron ore

Parameter	Simulation value
Internal Frictional Angle, φ (degrees)	47 ± 3 (5% wb moisture content)
Internal Frictional Angle, φ (degrees)	45 ± 3 (8% wb moisture content)
Cohesive Stiffness, $k_{adh}\left(\frac{N}{m}\right)$	$3.56\ x\ 10^8$ (5% wb moisture content)
Cohesive Stiffness, $k_{adh}\left(\frac{N}{m}\right)$	$5.93\ x\ 10^8$ (8% wb moisture content)
Wall Friction Angle, φ (degrees)	35 ± 3 (5% wb moisture content)

6 CONCLUSION

Numerous methods for material testing were presented to assist in the calibration process of the material parameters needed in DEM simulations. In this study, numerical results for cohesive granular material was compared to experimental data of copper ore at varying moisture content levels. The DEM parameters such as frictional coefficients and cohesive stiffness were varied until acceptable material conditions were met. The developed technique has proven to be successful in our projects involving the transfer of dry granular materials and has shown promising results in the calibration of cohesive materials. For full implementation of this method, optimizing simulation time would aid the computational cost. Further investigation is being conducted to access the validity and accuracy of our approach to DEM material characterization for cohesive granular materials.

8 REFERENCES

[1] L. Del Cid and G. Mustoe, “A Discrete Element Analysis of Cohesive Granular Bulk Solids Materials”, Proceedings of the IV Int. Conf. on Particle-Based Methods –

Fundamentals and Applications, 237-247 (2015).
[2] L. Del Cid (2015). A Discrete Element Methodology for the Analysis of Cohesive Granular Bulk Solid Materials (Doctoral dissertation). Colorado School of Mines.
[3] C.J. Coetzee, and D.N.J Els, "Calibration of Granular Material parameters for DEM Modelling and Numerical Verification by Blade-Granular Material Interaction", Journal of Terramechanics, 46 (2009) 15-26.
[4] C.J. Coetzee, and D.N.J. Els, "Calibration of Discrete Element Parameters and the Modelling of Silo Discharge and Bucket Filling", Computer and Electronics in Agriculture 65 (2009) 198-212.
[5] C.J. Coetzee, D.N.J Els, and G.F. Dymond, "Discrete Element Parameter Calibration and the Modelling of Dragline Bucket Filling", Journal of Terramechanics, 47 (2009) 33-44.
[6] Antony S. J., W. Hoyle, and Y. Ding. Granular materials: fundamentals and applications. Royal Society of Chemistry, 2004.
[7] Brown R. L. and J. C. Richards. Principles of powder mechanics. 1970.
[8] Radjaï F., F. Dubois, et al. Discrete-element modeling of granular materials. Wiley, 2011.
[9] Johnson K.L., K. Kendall, and A. D. Roberts. Surface energy and the contact of elastic solids. Proceedings of the Royal Society of London. A. mathematical and physical sciences, 324(1558):301-313, 1971.
[10] Lian G., C. Thornton, and M. J. Adams. A theoretical study of the liquid bridge forces between two rigid spherical bodies. Journal of Colloid and Interface Science, 161(1): 138{147, 1993.
[11] Gröger T., U. Tüzün, and D. M. Heyes. Modelling and measuring of cohesion in wet granular materials. Powder Technology, 133(1):203-215, 2003.
[12] Thakur S., J. P. Morrissey, J. Sun, J. F. Chen, and J. Y. Ooi. Particle scale modelling of cohesive powders for bulk handling applications. In EDEM Conference, 2011.
[13] da Cruz F., S. Emam, M. l. Prochnow, J. N. Roux, and F. Chevoir. Rheophysics of dense granular materials: Discrete simulation of plane shear flows. Physical Review E, 72(2):021309, 2005.
[14] Savage S. B. The mechanics of rapid granular flows. Advances in applied mechanics, 24:289-366, 1984.
[15] A. Grima and P. Wypych, "Development and Validation of Calibration Methods for Discrete Element Modelling", Granular Matter 13 (2011) 127-132.
[16] Schulze D. Flow properties of powders and bulk solids. Braunschweig/Wolfenbu ttel, Germany: University of Applied Sciences, 2006.
[17] Jenike A. W. Storage and ow of solids, bulletin no. 123. Bulletin of the University of Utah, 53(26), 1964.
[18] Schulze D. Development and application of a novel ring shear tester. Aufbereitungs-technik, 35(10):524-535, 1994.
[19] Schulze D. A new ring shear tester for flowability and time consolidation measurements. In Proc. 1st International Particle Technology Forum, pages 11-16, 1994
[20] Standard ASTM. D6773-02: Standard shear test method for bulk solids using the Schulze ring shear tester, ASTM international.